# Communication

## Single-Glass-Layer Optically Transparent Transmitarray With High Aperture Efficiency and Low Profile at 5G Millimeter-Wave Band

Byeongjin Kim and Jungsuek Oh

***Abstract*— This communication presents a single-glass-layer optically transparent transmitarray (TTA) with high aperture efficiency at millimeter-wave (mmWave) 5G band. When designing a transmitarray (TA), the more metal and dielectric layers are used, the easier it is to increase the aperture efficiency. However, if the TTA is designed, the fewer metal and dielectric layers, the more advantageous it is in terms of optical transparency (OT). Therefore, only a single glass layer was chosen to design a TTA with high OT. The novel analysis technique was applied to obtain the theoretical transmission response of the single substrate unit cell (UC) and to obtain impedance information to quickly design UCs by combining circuit analysis. Then, the aperture efficiency was increased using two methods: 1) two types of double resonance UCs were combined and 2) oblique incidence on the UCs on the edge of TA aperture was considered. The designed TA was converted into the TTA, which satisfies the advanced OT guidelines proposed in this communication. The fabricated TTA has a focal length (F) to dimension (D) ratio of 1.2, exhibiting simulated and measured aperture efficiencies of 51.1% and 45.3%.**

***Index Terms*— Aperture efficiency, millimeter-wave (mmWave), optical transparency (OT), transmitarray (TA), transparent transmitarray (TTA).**

### I. Introduction

Several years ago, millimeter-wave (mmWave) 5G communication was commercialized. Because of high transmission loss, mmWave 5G communication requires high-gain antennas [1], [2], [3], [4], [5]. Transmitarrays (TAs) feature low RF loss and no blockage loss. Currently, transmissive metasurfaces have been actively studied for various applications [6], [7], [8], [9], [10], [11], [12]. The visibility of such metasurfaces can be minimized if they are optically transparent [6], [9], [10], [11], [12]. In particular, transparent TAs (TTAs) can support 5G mmWave communication networks when they are integrated with the glass windows of buildings, vehicles, and displays.

To design a TTA, the substrates and metal patterns should be optically transparent [6], [9], [10], [11], [12]. Furthermore, fewer transparent conductor and dielectric layers are preferred, because they are not perfectly transparent [13]. However, at least three metal layers are required to obtain the full 360° phase tunable range when the multilayer frequency selective surfaces (M-FSSs) approach is utilized [14].

Manuscript received 12 May 2023; revised 31 July 2023; accepted 6 August 2023. Date of publication 21 August 2023; date of current version 30 October 2023. This work was supported by the Institute of Information and Communications Technology Planning and Evaluation (IITP) through the Korean Government [Ministry of Science and ICT (MSIT)] (Millimeter-Wave Metasurface-Based Dual-Band Beamforming Antenna-on-Package Technology for 5G Smartphone) under Grant 2020-0-00858. *(Corresponding author: Jungsuek Oh.)*

The authors are with the Institute of New Media and Communications (INMC), Department of Electrical and Computer Engineering, Seoul National University, Seoul 08826, South Korea (e-mail: jungsuek@snu.ac.kr).

Color versions of one or more figures in this article are available at https://doi.org/10.1109/TAP.2023.3305876.

Digital Object Identifier 10.1109/TAP.2023.3305876

Despite the inherent limit in the phase-tunable range, various TAs with double metal layers have been proposed [15], [16], [17], [18], [19], [20], [21], [22], [23], [24]. The metallic vias were embedded to achieve a wide phase-tunable range [15], [16], [17]. However, vias cannot be made transparent. Some of the others without via are covered with excessive metal [18], [19], [20], making them unsuitable for TTA design. The rest utilized the polarization conversion technique to obtain a wide phase-tunable range [21], [22], [23], [24]. However, these TAs are single-polarized; hence, they are not suitable for mmWave 5G communication, which requires high data rates.

In this communication, for the first time, TTA using a single glass layer was designed, achieving the highest aperture efficiency and high optical transparency (OT), at the 5G mmWave band. Although conventional TAs were often composed of over three metal and dielectric layers to achieve high aperture efficiency, only one glass layer was utilized in this communication for high OT. The high-aperture-efficiency TA was first designed with filled copper patterns and was converted into an equivalent mesh-grid TTA.

### II. Transmission Response Analysis and Quick Design of UCs With Single Substrate

#### A. Transmission Response of UCs With Single Substrate

Initially, the TA composed of filled copper patterns was designed. The authors aimed to design a single-glass-layer TTA for high OT. The use of via was excluded because vias cannot be made transparent and they are expensive for glasses.

To begin with, the impedance of a metal layer is denoted as $Z = jX$. Then, the multiple reflection method was applied to derive the total transmission response of unit cells (UCs) with a single substrate as a function of $Z$. In Fig. 1, transmission response patterns of UCs under various conditions are plotted. In the polar plot, the transmission magnitude and phase of one arbitrary UC corresponds to one point in the plot. The magnitude grows from 0 to 1 as the point locates farther from the center, and the phase can be read from the angle lines.

The UC type with a single metal layer shows a transmission response pattern of a circle according to the impedance of the metal layer, as shown in Fig. 1(a). Its phase tunable range is limited to only 90° when the 3-dB loss criterion is adopted. Fig. 1(b) and (c) shows that phase tunable range of double-metal-layer UCs enlarges when the electrical thickness of dielectric $kd$ decreases from 90°. However, as the thickness decreases, the number of points on the left circle of the pattern decreases, implying that the transmission response becomes highly sensitive to the impedance of metal patterns. For example, the transmission phase changes by up to 40° when the impedance changes by 1j Ω in the left circle of the pattern for the case of $kd = 15°$. This super-high sensitivity on impedance results in vulnerability to fabrication errors and also a narrow bandwidth. Finally, UCs with two identical metal layers are sufficient to cover the outermost line of the transmission patterns, implying the unnecessity

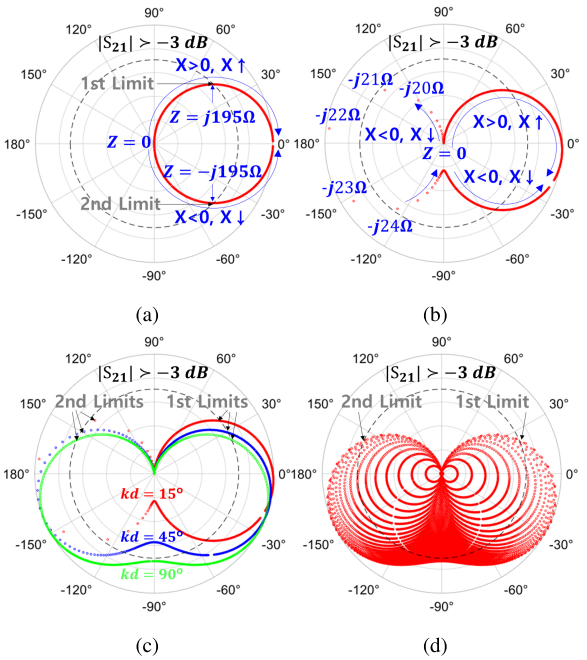


Fig. 1. Transmission response patterns of single- or double-metal-layer UCs with normal incidence at 28 GHz, assuming Z = jX (Ω). (a) Single-metal-layer UCs ($-10^4 < X < 10^4$, interval 1). Double-metal-layer UCs with glass ($\epsilon_r = 5.27$) substrate, (b) identical metal layers ($-10^4 < X_1 = X_2 < 10^4$, interval 1, $kd = 15°$), (c) identical metal layers ($-10^4 < X_1 = X_2 < 10^4$, interval 1, $kd = 15, 45, 90°$), and (d) different metal layers ($-10^4 < X_1, X_2 < 10^4$, interval 10, $kd = 90°$).

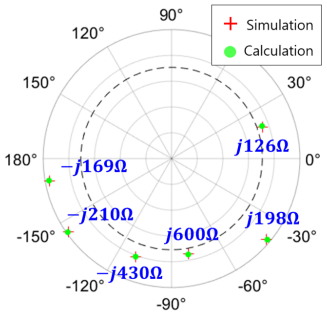


Fig. 2. Comparison of the calculated [by (7)–(14)] and simulated (by HFSS) transmission coefficients of UCs with two identical metal layers of several impedances and a glass layer ($\epsilon_r = 5.27$) with a normal incidence at 28 GHz.

of considering UCs with two different metal layers, as shown in Fig. 1(d).

Based on the discussions thus far, TTA's UCs were determined to be composed of double identical metal layers. Moreover, the authors chose the electrical thickness of the glass substrate as 1.2 mm, which is about 92.6°, for the stability of the design. The calculated and EM simulated transmission responses for several impedances are in good agreement, as shown in Fig. 2. The proposed transmission response analysis technique has a strong advantage compared to [14], such that one can determine the required impedance of metal layers to obtain the desired transmission response.

### *B. Quick Determination of UC Design Parameters*

Fig. 3 shows two types of UCs utilized in the design of the proposed TA. They are named as double-ring-type UC (DRUC) and ring-added patch-type UC (RPUC). The equivalent circuits of DRUC and RPUC are shown in Fig. 4. The equations for calculating the

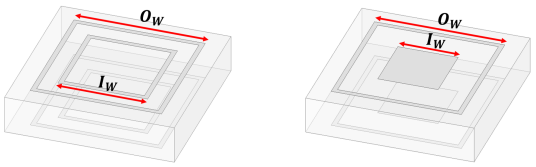


Fig. 3. Two types of UCs composing the proposed TTA. (a) DRUC and (b) RPUC.

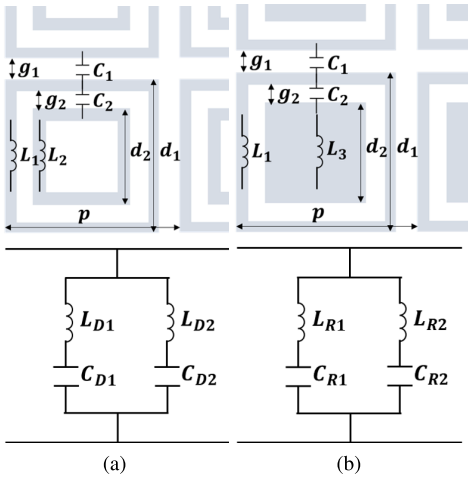


Fig. 4. Equivalent circuits of (a) DRUC and (b) RPUC.

circuit elements of DRUC are as follows [25], [26]:

$$\omega L_{D1} = \frac{2Z_0}{1/L_1 + 1/L_2} * \frac{d_1}{p}, \quad \omega C_{D1} = 0.75 * \frac{C_1}{Z_0} * \frac{d_1}{p}$$
$$\omega L_{D2} = Z_0 * L_3 * \frac{d_2}{p}, \quad \omega C_{D2} = \frac{1}{Z_0} * \frac{1}{1/C_1 + 1/C_2} * \frac{d_2}{p} \quad (1)$$

where

$$L_1 = F(p, w_1, \lambda), \quad L_2 = F(p, w_2, \lambda), \quad C_1 = 4F(p, g_1, \lambda)$$
$$L_3 = F(p, 2w_1, \lambda), \quad C_2 = 4F(p, g_2, \lambda) \quad (2)$$

where

$$F(p, s, \lambda) = \frac{p}{\lambda}\left(ln\, csc\frac{\pi s}{2p} + G(p, s, \lambda)\right)$$
$$p = 5.3 \text{ mm}, \quad w_1, w_2 = 0.15 \text{ mm}$$
$$g_1 = p - O_W, \quad g_2 = \frac{O_W - I_W - 2w_1}{2} \quad (3)$$

and the correction term $G(p, s, \lambda)$ can be found in [26]. $\lambda$ in (1)–(3) is the guided wavelength, which is the free space wavelength divided by the square root of the effective permittivity, except for $\lambda$ in $G(p, s, \lambda)$ terms of $L_1$, $L_2$, and $L_3$ [26]. For the latter, $\lambda$ is the free space wavelength. The effective permittivity is equal to $0.5(\epsilon_r + 1)$, where $\epsilon_r$ is the permittivity of the substrate layer [27].

The equations for calculating the circuit elements of RPUC were derived by the authors. $C_{R1}$, $L_{R2}$, and $C_{R2}$ correspond to $C_{D1}$, $L_{D2}$, and $C_{D2}$, respectively, but

$$L_3 = F(p, d_2, \lambda), \quad \omega L_{R1} = Z_0 * L_1 * d_1/p. \quad (4)$$

Once the impedance $Z$ of the UC that has a desired transmission response is calculated by multiple reflection method, design parameters $O_W$ and $I_W$ of DRUC and RPUC can be quickly derived by (1)–(4) without a laborious parametric study of full-wave EM simulations. For example, six UCs that have distinct desired transmission responses were designed by calculation and then optimized by the EM simulation, as shown in Table I. Calculated

TABLE I
UC DESIGN EXAMPLES USING THE NOVEL DESIGN METHOD

| UC# | Type | Desired $\angle S_{21}$ (°) | Calculated required impedance Z (Ω) | Calculated $(O_W, g_2)$ (mm, mm) | Optimized $(O_W, g_2)$ (mm, mm) by HFSS |
|---|---|---|---|---|---|
| 1 | RPUC | -170 | -j169 | (4.3, 0.79) | (4.3, 1.03) |
| 2 | RPUC | -145 | -j210 | (4.9, 1.30) | (4.9, 1.32) |
| 3 | RPUC | -110 | -j430 | (4.3, 1.21) | (4.3, 1.14) |
| 4 | RPUC | -80 | j600 | (3.7, 1.69) | (3.7, 1.33) |
| 5 | DRUC | -40 | j198 | (3.7, 0.22) | (3.7, 0.22) |
| 6 | DRUC | 20 | j126 | (3.9, 0.47) | (3.9, 0.44) |

design parameters agree well with the simulation, proving the validity of the proposed technique. UCs #1 and #4 show relatively large deviations because of their high sensitivity to the impedance at the desired transmission phases.

## III. DESIGN PROCEDURE OF SINGLE-GLASS-LAYER TA WITH HIGH APERTURE EFFICIENCY

### A. Combination of DRUC and RPUC

In practice, the actual phase tunable range that can be covered in the entire theoretical range is limited according to the shape of the metal pattern. DRUC and RPUC were considered as candidates because they operate with a dual resonance. Moreover, RPUC differs from DRUC only if the center of the inner ring is filled, enabling high similarity between adjacent UCs when arranged on the TA aperture, which reduces the error in the TA simulation [28]. Furthermore, both UC types have a small metal area and thus, a high OT inherently. The EM simulated transmission response pattern of DRUC shows a smaller size and a higher sensitivity (scarce points) in the left circle than the theoretical pattern, as shown in Fig. 5(a). This results in a higher transmission loss and a phase tunable range of 174°, which is considerably smaller than the theoretical range of 229°. The scarce number of points in the left circle also results in a higher sensitivity regarding the fabrication error. Meanwhile, the other element, RPUC showed a symmetrical pattern with DRUC, i.e., a bigger size and a lower sensitivity in the left circle as opposed to DRUC, as shown in Fig. 5(b). Therefore, DRUC and RPUC compensate for each other's transmission patterns when combined. When combined together, the two UC types can obtain the entire phase tunable range of 196°.

Notably, one can determine which UC metal pattern will result in a bigger left or right circle in the transmission pattern, without substantial EM parametric analysis. To this end, test UCs with transmission phases of −150° and −30° should be designed by the proposed technique in Section II-B and then optimized by HFSS. Then, it can be assumed that the test UC type has a bigger left circle pattern if the transmission loss of −150° UC is smaller than that of −30° UC, and vice versa.

### B. Special Consideration of Oblique Incidence on UCs on the Edge of TA Aperture

In previous studies, the transmission response of TA UCs was desired to be as insensitive as possible to the incidence angle to ignore the effect of the oblique incidence on the UC which is located on the edge of the TA aperture. However, variation in the transmission response according to the incidence angle cannot be perfectly removed. For example, for the proposed TA with 12 × 12 UCs and a focal length (F) to dimension (D) ratio of 1.2, 48 out of the total 144 UCs on the edge of the aperture receive 23°–31° oblique incidence wave. Fig. 6 shows that UCs assumed to have certain transmission phases under normal incidence conditions

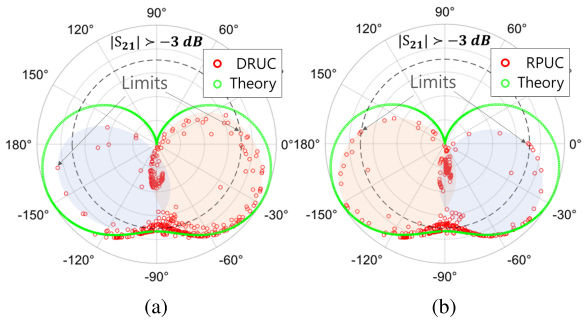


Fig. 5. EM simulated transmission coefficients of DRUC and RPUC at normal incidence, at 28 GHz. $O_W$ and $R_{OI} = (I_W/O_W)$ were swept from 0.5 to 5.1 mm and 0.3 to 0.8, respectively, and simultaneously. (a) DRUC and (b) RPUC.

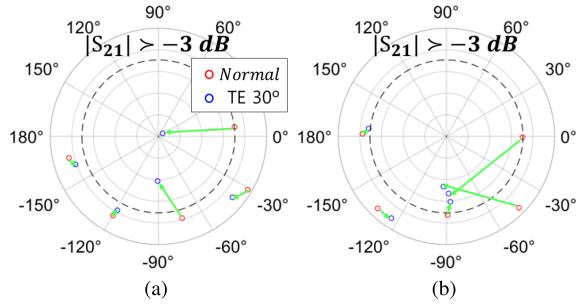


Fig. 6. Demonstration of distorted transmission responses without consideration of oblique incidence on the UCs on the edge of the TA aperture, at 28 GHz. (a) DRUC from normal to 30° TE oblique incidence. (b) RPUC from normal to 30° TE oblique incidence.

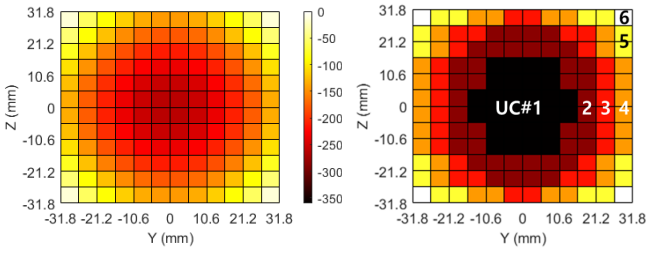


Fig. 7. (a) Phase distribution in the TA. (b) UC arrangement.

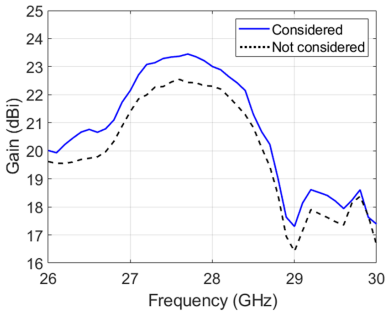


Fig. 8. Peak gain comparison of TAs with and without consideration of oblique incidence on the UCs on the edge of the aperture.

have completely different transmission phases under 30° TE oblique incidence conditions. Similar results were obtained with 30° TM oblique incidence conditions. The TA designed without considering such error loses accuracy during phase compensation by UCs on the edge of the aperture and results in a lower aperture efficiency. The final phase tunable range considering the oblique incidence is 210°.

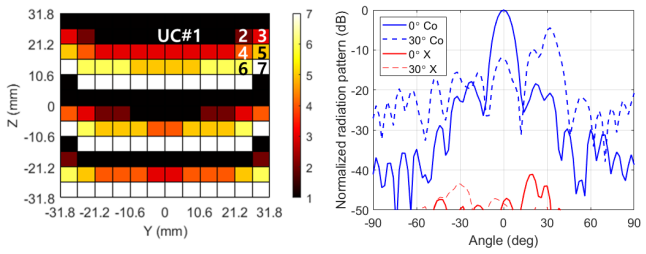


(a) (b)

Fig. 9. (a) UC arrangement of the 30° tilted beam TA. (b) H-plane radiation patterns of 0° and 30° tilted beam TAs.

Finally, a TA was designed to confirm the validity of the proposed aperture efficiency-increasing methods. The EAGLE XG glass ($\epsilon_r = 5.27$, $\delta = 0.003$) with a thickness of 1.2 mm was chosen as a single glass substrate. A $Ka$-band horn antenna was chosen as the feed antenna. Following the calculation method introduced in [29], D = $6\lambda$ and F/D = 1.2 were chosen to maximize the aperture efficiency. The TA consists of 12 × 12 UCs with a UC size of 5.3 × 5.3 mm, which is half the wavelength. Six types of UCs among DRUC and RPUC with a phase-tuning interval of 30°–45° were used in the TA design, following the arrangement method introduced in [30]. The required phase distribution on the TA aperture obtained by EM simulation and the corresponding UC arrangement are shown in Fig. 7. The information about UCs #1–#6 is listed in Table I. UC #1 which is exhibiting a phase shift of −172° was chosen to maximize aperture efficiency. That is, by giving up a phase range of 20°, the transmission loss is reduced from 3 to 1.2 dB. The simulated peak gain of TAs with and without considering oblique incidence on the UCs on the edge of the TA aperture is compared in Fig. 8. The peak gain of TA increased by 0.91 dB, from 22.54 to 23.45 dBi, and aperture efficiency increased by 9.4%, from 41.7% to 51.1%. Finally, Fig. 9 shows the UC arrangement for the 30° tilted beam TA and H-plane radiation patterns of 0° and 30° tilted beam TAs. The 30° TA showed a peak gain of 19.0 dBi. It exhibited a relatively high sidelobe level (SLL) because of the limited phase tunable range and higher UC inhomogeneity on the TA aperture.

## IV. Conversion to the Optically Transparent TA

### A. Advanced Definition of OT

The OT can be either measured or calculated theoretically. It is calculated as the nonmetal-filled area-to-total area ratio for a metal mesh. However, the OT will be calculated as good if an arbitrarily large blank area is set, regardless of the density and thickness of the linewidth of the metal mesh. Therefore, the current definition of OT should be supplemented by carefully defining the total area and setting the upper limit of the linewidth of the metal mesh. First, the concepts of the UCOT and pattern OT (POT) should be differentiated by properly defining the total area. UCOT represents the original definition of OT used in [11], while POT considers the total area of the mesh-grid pattern itself, including the gaps between thin lines. POT larger than 75% may be used as a guideline as many countries have regulations requiring the OT of at least 70% for the front windshield of a vehicle [6].

Second, the authors propose the use of visual acuity (VA) to set the upper limit of the linewidth of the metal mesh. VA refers to the degree of spatial resolution of human vision [31]. VA in Snellen notation is calculated as follows:

$$VA = \frac{1}{MAR} \tag{5}$$

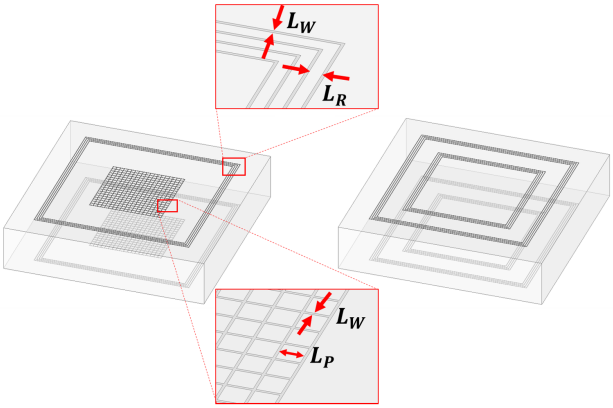


Fig. 10. Equivalently converted optically transparent UCs and their mesh-grid components in the enlarged view.

TABLE II
UC OTs and Response Variation in Conversion Procedure Designs

| Unit Cell # | $\Delta\lvert S_{21}\rvert$ (dB) | $\Delta(\angle S_{21})$ (°) | POT (%) | UCOT (%) |
|---|---|---|---|---|
| 1 | -0.6 | +4 | 78.5 | 95.5 |
| 2 | -0.3 | +5 | 78.0 | 95.2 |
| 3 | -0.5 | -1 | 78.0 | 95.7 |
| 4 | -0.3 | 0 | 77.9 | 97.4 |
| 5 | +0.5 | +3 | 87.5 | 98.1 |
| 6 | -0.4 | +3 | 75.0 | 96.3 |

where MAR is the minimum angular resolution. If a person can resolve minimum angular width of one arcminute at a distance of 6 m, MAR = 1 and VA = 1/1 = 6/6. A VA of 6/6 is considered to have normal vision, and 6/3 is considered to have good vision. When human eyes with VAs of 6/6, 6/3, and 2.5 are 10 cm away from the object, which is a moderately close distance, they cannot resolve spacings of less than 29, 14.5, and 11.6 $\mu$m, respectively, according to (5). Therefore, the upper limit of the linewidth of the metal mesh being 11 $\mu$m is acceptable for general purposes.

### B. Equivalent Optically Transparent UCs

Two types of UCs, RPUC and DRUC, were converted into equivalent mesh-grid UCs to design the proposed TTA. The ring and patch in both RPUC and DRUC can be equivalently converted as a composite of concentric rings and a mesh-grid patch, respectively, as shown in Fig. 10, after optimization. The linewidth of the metal mesh in both types of UCs ($L_W$) was set to 10 $\mu$m. The gaps between the concentric rings ($L_R$) were set to 40 $\mu$m to satisfy the POT condition. The gaps between the thin lines ($L_P$) of the cross-mesh formed patch were set as 90–95 $\mu$m, resulting in a patch POT larger than 80%. An optimization process was done to obtain a similar transmission response to the original UCs. All UCs exhibited variation in the transmission loss and the phase shift of less than 1 dB and 5° when they were converted to equivalent mesh-grid UCs, as presented in Table II. Furthermore, all the mesh-grid UCs exhibited a POT and UCOT larger than 75% and 95%, respectively, satisfying sufficient levels for both optical transparencies.

## V. Fabrication and Measurement Results With Discussion

The thickness of mesh-grid metal patterns must be limited to several hundreds of nanometers, to guarantee OT. Therefore, several metal thicknesses were tested for the meshed UCs to find the optimal thickness, as shown in Table III. The metal thickness was

TABLE III
UC TRANSMISSION LOSS ACCORDING TO METAL THICKNESS

| Metal thickness ($\mu$m) | #1 | #2 | #3 | #4 | #5 | #6 |
|---|---|---|---|---|---|---|
| 18 | 1.5 | 0.75 | 2.1 | 2.8 | 0.5 | 2.9 |
| 0.3 | 1.8 | 1.0 | 2.2 | 3.0 | 0.7 | 3.1 |
| 0.2 | 2.3 | 1.4 | 2.4 | 3.2 | 1.1 | 3.5 |

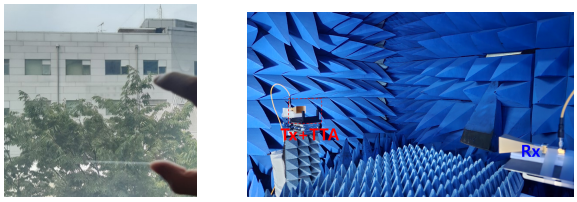


(a) (b)

Fig. 11. Photographs of (a) fabricated TTA sample with the background and (b) measurement setup in an anechoic mmWave RF chamber in Seoul National University.

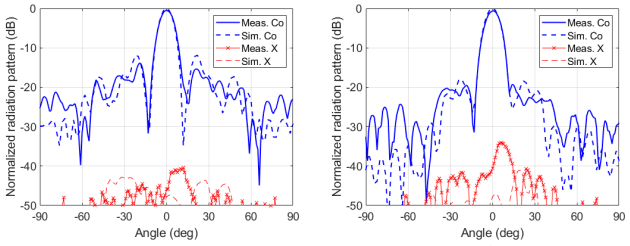


(a) (b)

Fig. 12. Simulated (at 27.7 GHz) and measured (at 28.4 GHz) E- and H-plane normalized radiation patterns. (a) E-plane and (b) H-plane.

TABLE IV
LOSS BUDGET OF THE PROPOSED TTA AT 28.4 GHZ

| | |
|---|---|
| Ideal directivity | 26.6 dBi |
| Return loss | 0.10 dB |
| Spillover loss | 0.56 dB |
| Taper loss | 0.71 dB |
| Phase error loss | 0.69 dB |
| TA insertion loss | 1.33 dB |
| Dielectric and conductive losses | 0.27 dB |
| Measured gain | 22.9 dBi |

determined as 300 nm. The photograph of the fabricated sample with a background [Fig. 11(a)] proves that the proposed advanced OT concept and conversion procedure guarantee minimum visual impact.

The measurement setup is illustrated in Fig. 11(b). The simulated and measured E- and H-plane radiation patterns are shown in Fig. 12. The proposed TTA could not be simulated because of the long simulation time owing to its fine mesh structure. Therefore, a filled-copper TA was simulated to provide the simulation results. The good agreement in the simulated and measured radiation patterns indicates that the conversion process from TA to TTA was successful. The simulated and measured peak gains were 23.45 and 22.89 dBi at 27.7 and 28.4 GHz, respectively. The peak gain frequency was slightly shifted because of the conversion process of the UC and the fabrication errors. The simulated and measured aperture efficiencies were 51.1% and 45.3%, respectively. Major losses degrading the aperture efficiency are listed in Table IV. They were calculated by equations and HFSS [32]. The simulated and measured radiation efficiencies were 94.0% and 74.5%, respectively. The E- and H-plane SLLs were simulated and measured as −11.9 and −13.8 dB, and −17.9 and −19.3 dB, respectively. The relatively high E-plane SLL is obtained from the limited phase tunable range, a few different UCs and a few entire UCs composing the proposed TA [18], [33], [34]. The performance comparison between the TTAs and single substrate nonvia TAs is presented in Table V.

TABLE V
COMPARISON OF THE PROPOSED TTA WITH OTHER TA DESIGNS

| Ref. | Frequency (GHz) | Gain (dBi) | Aperture efficiency (%) | OT (%) | Total thickness ($\lambda_0$ *) |
|---|---|---|---|---|---|
| [6] | 28 | 25.4 | 0.5 | >89.8 | 0.09 |
| [11] | 28.5 | 25 | 32.3 | N/A | 0.57 |
| [12] | 12 | 20.22 | 33.0 | N/A | 0.32 |
| [18] | 6 | 16.7 | 23.4 | 0 | 0.28 |
| [19] | 60.5 | 33.1 | 42.1 | 0 | 0.10 |
| [20] | 10 | 15.7 | 24.6 | 0 | 0.10 |
| This work | 28.4 | (Sim.) 23.45 (Meas.) 22.89 | (Sim.) 51.1 (Meas.) 45.3 | 96.1 | 0.11 |

* $\lambda_0$ is the free space wavelength at the frequency.

## VI. CONCLUSION

A single-glass-layer 5G mmWave TTA achieving the highest aperture efficiency and high OT was proposed. Only a single glass layer was utilized for high OT. The novel technique was applied to analyze the transmission response of UCs and for the quick UC design by combining it with the circuit analysis. To achieve a high aperture efficiency, two techniques were devised. Furthermore, advanced OT concepts were proposed. Finally, the generalized conversion method from the filled-copper TA to the mesh-grid TTA was verified by the good agreement in the simulated and measured results.

## REFERENCES

[1] J. Seo et al., "Miniaturized dual-band broadside/endfire antenna-in-package for 5G smartphone," *IEEE Trans. Antennas Propag.*, vol. 69, no. 12, pp. 8100–8114, Dec. 2021.

[2] D. Seo, H. Kim, S. Oh, J. Kim, and J. Oh, "Ultrathin high-gain D-band transmitarray based on a spatial filter topology utilizing bonding layer effect," *IEEE Antennas Wireless Propag. Lett.*, vol. 21, no. 10, pp. 1945–1949, Oct. 2022.

[3] H. Kim, J. Kim, and J. Oh, "Liquid-crystal-based X-band reactively loaded reflectarray unit cell to reduce reflection loss," *IEEE Antennas Wireless Propag. Lett.*, vol. 20, no. 10, pp. 1898–1902, Oct. 2021.

[4] I. Kim and B. Lee, "Wideband antenna for high-frequency 5G wireless communication," *J. Electromagn. Eng. Sci.*, vol. 22, no. 3, pp. 296–301, May 2022.

[5] T. Joo, C. Hwang, J. Park, K. Kim, and J. Jung, "Design of a tile-type Rx multi-beam digital active phased array antenna system," *J. Electromagn. Eng. Sci.*, vol. 22, no. 1, pp. 12–20, Jan. 2022.

[6] D. Kitayama et al., "Transparent dynamic metasurface for a visually unaffected reconfigurable intelligent surface: Controlling transmission/reflection and making a window into an RF lens," *Opt. Exp.*, vol. 29, no. 18, pp. 29292–29307, Aug. 2021.

[7] H. Kim and S. Nam, "Transmission enhancement methods for low-emissivity glass at 5G mmWave band," *IEEE Antennas Wireless Propag. Lett.*, vol. 20, no. 1, pp. 108–112, Jan. 2021.

[8] S. Hong, Y. Kim, and J. Oh, "Automobile laminated glass window embedded transmitarray and ray tracing validation for enhanced 5G connectivity," *IEEE Trans. Antennas Propag.*, vol. 70, no. 8, pp. 6671–6682, Aug. 2022.

[9] P. Zhang, X. Zhang, and L. Li, "An optically transparent metantenna for RF wireless energy harvesting," *IEEE Trans. Antennas Propag.*, vol. 70, no. 4, pp. 2550–2560, Apr. 2022.

[10] J. Chen, Y. Wei, Y. Zhao, L. Lin, L. Li, and T. Su, "Transparent and broadband diffusion metasurface with high transparency and high shielding effectiveness using metallic mesh," *IEEE Trans. Antennas Propag.*, vol. 70, no. 7, pp. 5574–5583, Jul. 2022.

[11] G. Liu, M. R. D. Kodnoeih, K. T. Pham, E. M. Cruz, D. González-Ovejero, and R. Sauleau, "A millimeter-wave multibeam transparent transmitarray antenna at Ka-band," *IEEE Antennas Wireless Propag. Lett.*, vol. 18, no. 4, pp. 631–635, Apr. 2019.

[12] N. A. Al-Shalaby and S. M. Gaber, "Parametric study on effect of solar-cell position on the performance of transparent DRA transmitarray," *AEU-Int. J. Electron. Commun.*, vol. 70, no. 4, pp. 436–441, Apr. 2016.

[13] K. Nattermann, N. Neuroth, and R. J. Scheller, *he Properties of Optical Glass*. Cham, Switzerland: Springer, 1998.

[14] A. H. Abdelrahman, A. Z. Elsherbeni, and F. Yang, "Transmission phase limit of multilayer frequency-selective surfaces for transmitarray designs," *IEEE Trans. Antennas Propag.*, vol. 62, no. 2, pp. 690–697, Feb. 2014.

[15] X. Yi, T. Su, X. Li, B. Wu, and L. Yang, "A double-layer wideband transmitarray antenna using two degrees of freedom elements around 20 GHz," *IEEE Trans. Antennas Propag.*, vol. 67, no. 4, pp. 2798–2802, Apr. 2019.

[16] S. Yang, Z. Yan, M. Cai, F. Fan, and T. Zhang, "A high-efficiency double-layer transmitarray antenna using low-loss dual-linearly polarized elements," *IEEE Antennas Wireless Propag. Lett.*, vol. 19, no. 12, pp. 2378–2382, Dec. 2020.

[17] W. Hu et al., "A wideband metal-only transmitarray with two-layer configuration," *IEEE Antennas Wireless Propag. Lett.*, vol. 20, no. 7, pp. 1347–1351, Jul. 2021.

[18] Y. Chen, L. Chen, J.-F. Yu, and X.-W. Shi, "A C-band flat lens antenna with double-ring slot elements," *IEEE Antennas Wireless Propag. Lett.*, vol. 12, pp. 341–344, 2013.

[19] W. An, X. Zhang, Y. Luo, J. Wang, and L. Xiong, "60-GHz double-layer transmitarray antenna using complementary structure," *Frontiers Phys.*, vol. 10, pp. 1–10, Apr. 2022.

[20] H. Li, G. Wang, J. Liang, X. Gao, H. Hou, and X. Jia, "Single-layer focusing gradient metasurface for ultrathin planar lens antenna application," *IEEE Trans. Antennas Propag.*, vol. 65, no. 3, pp. 1452–1457, Mar. 2017.

[21] H. Yi, S. Qu, and C. H. Chan, "Low-cost two-layer terahertz transmit array," *Electron. Lett.*, vol. 53, no. 12, pp. 789–791, Jun. 2017.

[22] M. Euler and V. F. Fusco, "Frequency selective surface using nested split ring slot elements as a lens with mechanically reconfigurable beam steering capability," *IEEE Trans. Antennas Propag.*, vol. 58, no. 10, pp. 3417–3421, Oct. 2010.

[23] K. Liu, G. Wang, T. Cai, W. Guo, Y. Zhuang, and G. Liu, "Ultra-thin circularly polarized lens antenna based on single-layered transparent metasurface," *Chin. Phys. B*, vol. 27, no. 8, Aug. 2018, Art. no. 084101.

[24] X. Zhang, F. Yang, S. Xu, A. Aziz, and M. Li, "Dual-layer transmitarray antenna with high transmission efficiency," *IEEE Trans. Antennas Propag.*, vol. 68, no. 8, pp. 6003–6012, Aug. 2020.

[25] R. J. Langley and E. A. Parker, "Double-square frequency-selective surfaces and their equivalent circuit," *Electron. Lett.*, vol. 19, no. 17, pp. 675–677, Aug. 1983.

[26] N. Marcuvitz, *Waveguide Handbook*. Lexington, MA, USA: Boston Tech. Publishers, 1964.

[27] G. Sung, K. Sowerby, M. Neve, and A. Williamson, "A frequency-selective wall for interference reduction in wireless indoor environments," *IEEE Antennas Propag. Mag.*, vol. 48, no. 5, pp. 29–37, Oct. 2006.

[28] M-A. Milon, D. Cadoret, R. Gillard, and H. Legay, "Surrounded-element approach for the simulation of reflectarray radiating cells," *IET Microw., Antennas Propag.*, vol. 1, no. 2, pp. 289–293, Apr. 2007.

[29] A. Yu, F. Yang, A. Z. Elsherbeni, J. Huang, and Y. Rahmat-Samii, "Aperture efficiency analysis of reflectarray antennas," *Microw. Opt. Technol. Lett.*, vol. 52, no. 2, pp. 364–372, Feb. 2010.

[30] D. R. Smith, O. Yurduseven, L. P. Mancera, P. Bowen, and N. B. Kundtz, "Analysis of a waveguide-fed metasurface antenna," *Phys. Rev. Appl.*, vol. 8, no. 5, pp. 1–16, Nov. 2017.

[31] H. Kolb et al. (Jun. 5, 2007). *WebVision: The Organization of the Retina and Visual System*. [Online]. Available: https://webvision.med.utah.edu/

[32] X. Dai, G.-B. Wu, and K.-M. Luk, "A wideband circularly polarized transmitarray antenna for millimeter-wave applications," *IEEE Trans. Antennas Propag.*, vol. 71, no. 2, pp. 1889–1894, Feb. 2023.

[33] A. H. Abdelrahman et al., *Analysis and Design of Transmitarray Antennas*. San Rafael, CA, USA: Morgan & Claypool, 2017.

[34] F. Wu, J. Wang, R. Lu, X. Xia, W. Hong, and K.-M. Luk, "Wideband and low cross-polarization transmitarray using 1 bit magnetoelectric dipole elements," *IEEE Trans. Antennas Propag.*, vol. 69, no. 5, pp. 2605–2614, May 2021.